

Intercomparison of spatially distributed models for predicting surface energy flux patterns during SMACEX

Wade T. Crow, Fuqin Li, and William P. Kustas

USDA ARS, Hydrology and Remote Sensing Laboratory, Beltsville, MD

Short title: INTERCOMPARISON OF FLUX PATTERNS

Abstract. The treatment of aerodynamic surface temperature in surface vegetation atmosphere transfer (SVAT) models can be used to classify approaches into two broad categories. The first category contains models utilizing remote sensing (RS) observations of surface radiometric temperature to estimate aerodynamic surface temperature and solve the terrestrial energy balance. The second category contains combined water and energy balance (WEB) approaches that simultaneously solve for surface temperature and energy fluxes based on observations of incoming radiation, precipitation, and micro-meteorological variables. To date, few studies have focused on cross-comparing model predictions from each category. Land surface and remote sensing data sets collected during the 2002 Soil Moisture Atmosphere Coupling Experiment (SMACEX) provide an opportunity to evaluate and intercompare spatially distributed surface energy balance models. Intercomparison results presented here focus on the ability of a WEB-SVAT approach (the TOPmodel-based Land Atmosphere Transfer Scheme - TOPLATS) and a RS-SVAT approach (the Two-Source Energy Balance - TSEB - model) to accurately predict patterns of turbulent energy fluxes observed during SMACEX. During the experiment, TOPLATS and TSEB latent heat flux predictions match flux tower observations with a root-mean-square (RMS) accuracy of 67 and 63 Wm^{-2} , respectively. TSEB predictions of H are significantly more accurate with an RMS accuracy of 22 Wm^{-2} versus 46 Wm^{-2} for TOPLATS. Intercomparison of flux predictions from each model suggests that modeling errors for each approach are sufficiently independent that opportunities exist for improving the performance of both models via data assimilation and model calibration techniques that integrate RS-SVAT

and WEB-SVAT energy flux predictions.

1. Introduction

Within the past several decades, a large number of land surface models have been developed to predict the partitioning of surface net radiation between sensible and latent heating. These approaches are frequently lumped together under the broad category of surface vegetation atmosphere transfer (SVAT) schemes. Such broad terminology belies a number of key structural differences between approaches. For example, the contrasting treatment of surface temperature in SVAT models can be used to separate them into broad two categories.

The first category contains SVAT models utilizing remotely-sensed (RS) observations of surface radiometric temperature (T_s) to partition observations of net radiation (Rn) into various flux components. With a few exceptions (see e.g. Castelli et al., 1999), these approaches are diagnostic in nature and do not temporally integrate any surface state information. Instead, energy flux predictions are made for instantaneous times at which remote observations of T_s are available. RS-SVAT models are typically run at grid sizes corresponding to the spatial resolution of the remotely-sensed T_s measurements. This ranges from between 10-30 m for high-resolution airborne observations (French et al., 2003) to 8 km for operational approaches based on geostationary satellite measurements (Mecikalski et al., 1999). Examples of RS-SVAT models include: the Two-Source Energy Balance (TSEB) model (Norman et al., 1995), the Surface Energy Balance (SEBAL) model (Bastiaanssen et al., 1998), and the Surface Energy Balance System (SEBS) (Su et al., 2002).

The second broad SVAT model category consists of coupled water and energy balance (WEB) approaches containing prognostic equations for the temporal evolution of soil moisture and thermal states based on observed rainfall, micro-meteorology, and radiative forcings. In this framework, surface temperature is a predicted state and not a forcing variable. As opposed to RS-SVAT models, WEB-SVAT models are multi-objective in nature and make predictions of surface states (e.g. soil moisture) and water fluxes (e.g. runoff) in addition to partitioning the surface energy budget (Gupta et al., 1999). As a consequence they are typically more complex and heavily parameterized than RS-SVAT approaches. A key application for WEB-SVAT models is providing atmospheric prediction models with estimates of surface states impacting fluxes of heat, momentum, and water vapor between the land surface and boundary layer. This is accomplished either through direct coupling with the atmospheric model or through land data assimilation systems that provide operational off-line estimates of surface states derived from observations of precipitation and radiation (Rodell et al., 2003; Mitchell et al., 2004). WEB-SVAT models are often run at coarse grid-scales (10-100 km) to facilitate coupling with global and regional atmospheric models. However, their energy flux parameterizations are typically based on stomatal and aerodynamic conductance principles developed at much finer patch-scales (10-50 m). Examples of WEB-SVAT schemes include: the TOPmodel-based Land Atmosphere Transfer Scheme (TOPLATS) (Famiglietti and Wood, 1994; Peters-Lidard et al., 1997), the Variable Infiltration Capacity (VIC) model (Liang et al., 1994), the Common Land Model (CLM) (Dai et al. 2003), and the Catchment Land Surface model (Koster et al., 2000).

Intercomparison of WEB-SVAT schemes is an active area of research (Wood et al., 1998; Pitman et al., 1999; Henderson-Sellers et al., 2003). Intercomparison of RS-SVAT approaches, while less common, have also appeared in the literature (Zhan et al., 1996; Bindlish et al., 2001). However, despite the fact that both predict surface energy fluxes over similar scales, few studies have intercompared WEB- and RS-SVAT energy flux predictions. Such intercomparisons may prove illuminating since WEB- and RS-SVAT models arrive at energy flux predictions using different methodologies. In particular, the use of spatially explicit T_s observations to drive RS-SVAT energy flux predictions gives RS-SVAT models access to a critical land surface observation that is typically not by utilized WEB-SVAT approaches. Extensive surface energy flux measurements made during the 2002 Soil Moisture Atmosphere Coupling Experiment (SMACEX) (Kustas et al., this issue) provide an observational framework in which to undertake an intercomparison study aimed at examining spatial differences in WEB-SVAT and RS-SVAT energy flux predictions. One potential benefit of such comparisons is the design of data assimilation and/or calibration strategies to minimize WEB-SVAT soil moisture and energy flux errors via the incorporation of RS-SVAT model energy flux predictions.

The purpose of this analysis is two-fold. First, to intercompare spatially distributed predictions of surface energy fluxes made by a WEB-SVAT approach (TOPLATS) and a RS-SVAT approach (the TSEB model) to each other and extensive flux tower observations collected during the SMACEX field experiment. Second, to examine prospects for exploiting these intercomparisons to realize improvements in either model

via error filtering or model calibration techniques. Section 2 contains descriptions of both models. The application of models to the SMACEX study area is described in Section 3. Intercomparison results are presented in Section 4 and discussed in Section 5.

2. Model descriptions

RS- and WEB-SVAT models take contrasting approaches to the calculation of surface energy fluxes. Key contrasts and the specifics of the particular models employed here are described in the following two subsections.

2.1. RS-SVAT Modeling (TSEB)

A baseline strategy for many RS-SVAT approaches is to assume the availability of net radiation (Rn) observations, calculate ground heat flux (G) as a simple function of Rn and vegetation density, and estimate sensible heat (H) as:

$$H = \rho C_p \frac{T_{aero} - T_a}{R_a}, \quad (1)$$

where ρ is the density of air, C_p is the heat capacity of air, T_{aero} the aerodynamic surface temperature, T_a the air temperature and R_a is the surface aerodynamic resistance.

Latent heating (LH) is then calculated as a residual of the surface energy balance:

$$LH = Rn - H - G. \quad (2)$$

The approach is purely diagnostic and no prognostic predictions of surface thermal or moisture states are made. Vegetation water stress is diagnosed by monitoring daytime

differences between estimates of T_{aero} and observations of T_a . A fundamental problem with this baseline approach is that T_{aero} values required for (1) are a complex function of surface radiometric temperature observations (T_s), viewing angle, and vegetation characteristics for partial vegetation canopies (Kustas and Norman, 1996). In addition, typical uncertainties of 2-4 K in T_s observations hamper the accurate estimation of $T_{aero} - T_a$ gradients (Kustas and Norman, 1997). In response to these problems, a number of key improvements to this baseline strategy have been proposed. These include the use of contextual information in space to estimate surrogates for canopy resistance to transpiration (e.g. Bastiaanssen et al., 1998; Jiang and Islam, 2001), the coupling of approaches with a simplified boundary-layer model (Mecikalski et al., 1999), and the use of both multi-angular and multi-temporal T_s observations to reduce uncertainties in the estimation of $T_{aero} - T_a$ (Kustas and Norman, 1997; Anderson et al., 1997).

A key precursor to many of these advances was the development of two-source emission techniques to effectively disaggregate T_s observations into canopy and vegetation components. A detailed description of the original TSEB model can be found in Norman et al. (1995). The modeling approach evaluates the temperature contribution of the vegetated canopy layer and soil/substrate to the radiometric surface temperature observation, and the resulting turbulent heat flux contributions driven by surface-air temperature differences with aerodynamic resistance parameterizations for the vegetation and soil components. Rn is assumed to be observed and G is calculated as a simple fraction of Rn , leaf area index (LAI), and time of day (Kustas et al., 1998). Several modifications to the original TSEB formulation have been made which

can significantly influence flux predictions for partial canopy covered surfaces. These include estimating the divergence of net radiation through the canopy layer with a more physically-based algorithm, adding a simple method to address the effects of clumped vegetation on radiation divergence and wind speed inside the canopy layer, adjusting the magnitude of the Priestley-Taylor (Priestley and Taylor, 1972) coefficient used in estimating canopy transpiration, and formulating a new estimation for soil resistance to sensible heat flux transfer (Kustas and Norman, 1999ab; Kustas and Norman, 2000ab). See Li et al. (this issue) for a detailed description of current TSEB algorithms.

2.2. WEB-SVAT MODELING (TOPLATS)

Most WEB-SVAT approaches make energy flux predictions by parameterizing components of the surface energy balance (Rn , H , LH and G) as a function of: aerodynamic surface temperature (T_{aero}), static surface parameters describing soil and vegetation properties (\mathbf{P}), forcing variables (e.g. precipitation and incoming radiation) (\mathbf{W}), and current soil thermal (\mathbf{T}) and hydrologic states ($\mathbf{\Theta}$):

$$Rn(T_{aero}, \mathbf{P}, \mathbf{W}) = H(T_{aero}, \mathbf{P}, \mathbf{W}) + LH(T_{aero}, \mathbf{P}, \mathbf{W}, \mathbf{\Theta}) + G(T_{aero}, \mathbf{P}, \mathbf{W}, \mathbf{T}, \mathbf{\Theta}). \quad (3)$$

All parameters are assumed known and specified by the user, meteorological variables, including rainfall, are assumed to be measured, and current soil temperature and moisture states are calculated through the temporal propagation of prognostic equations:

$$d\mathbf{T}/dt = f(T_{aero}, \mathbf{\Theta}, \mathbf{T}, \mathbf{P}, \mathbf{W}) \quad (4)$$

$$d\Theta/dt = f(LH, \Theta, \mathbf{T}, \mathbf{P}, \mathbf{W}). \quad (5)$$

Some kind of numerical scheme is typically used to solve (3) for T_{aero} , Rn , LH , H , and G . T_{aero} and LH solutions are then used to explicitly update moisture and temperature states via (4) and (5). Coupling between the water and energy balance comes primarily from the modeled ability of soil moisture limitations to curb evaporation or transpiration rates to levels below atmospheric demand. Because T_s observations are not utilized, WEB-SVAT approaches rely on rainfall observations and (5) to detect soil moisture conditions conducive to water stress and water-limited evapotranspiration. Ground heat flux predictions are made by comparing surface temperature levels diagnosed via (3) and deeper soil thermal states (with greater memory) predicted via (4). The thermal characteristics of the soil are often modified based on soil moisture content predicted via (5).

Despite a common conceptual basis, WEB-SVAT models vary greatly in their specific parameterization of (3)-(5). These differences can lead to large contrasts in energy flux predictions (Henderson-Sellers et al., 2003) and make it difficult to broadly generalize WEB-SVAT results. The specific parameterization used here is based on the baseline version of the TOPLATS model described in Peters-Lidard et al. (1997), hereafter referred to as PL97, plus recent model modifications described in Crow et al. (2004).

For this analysis, TOPLATS crop pixels were conceptually divided into bare soil and vegetated components and separate energy balance calculations performed via

(3) on each sub-pixel surface. In the absence of canopy water storage, all LH in the vegetated fraction of the pixel is assumed due to plant transpiration ET and calculated as:

$$ET = \text{Min}(ET_p, \sum_{i=1}^4 \rho_i ET_{max_i}), \quad (6)$$

where ET_{max_i} is the maximum rate of transpiration sustainable given the moisture status of soil layer i , ρ_i is the relative fraction of root area within layer i , and ET_p the potential transpiration. ET_p is calculated, as a function of T_{aero} , using the Jarvis-type approach presented in PL97. ET_{max_i} is based on the approach of Wetzel and Chang (1988) and Famiglietti et al. (1994) where:

$$ET_{max_i} = \frac{\psi(\theta_i) - \psi_c}{r_s(\theta_i) + r_p}, \quad (7)$$

and ψ is the soil water matrix potential, θ_i is the soil moisture in layer i , ψ_c is the critical soil moisture potential at which plant wilting begins, r_s is the soil resistivity to water flow into the roots, and r_p the internal plant resistivity to water flow. The resistivity r_s is modeled as:

$$r_s = \alpha/K(\theta), \quad (8)$$

where α is a root geometry parameter and K is the hydraulic conductivity of the soil. Turbulent fluxes from bare soil surfaces are calculated using parameterizations listed in PL97 except, following Sauer et al. (1995), an additional resistance term is added to parameterize aerodynamic resistance to momentum flux beneath the vegetation canopy:

$$R_{a,soil} = (c'(T_{aero,veg} - T_{aero,soil}) + b'u_s)^{-1}, \quad (9)$$

where c' and b' are constants approximated as 0.0025 and 0.012, u_s is the wind speed near the soil surface, and T_{aero} (in degrees C) is calculated via (3). As in the TSEB model, u_s is approximated using the exponential model of Goudriaan (1977). This new resistance term is placed in series with an estimate of aerodynamic resistance above the canopy in order to calculate turbulent energy fluxes from bare soil surfaces.

Total grid cell energy flux g_T is calculated as a weighted average of fluxes predicted over vegetation (g_v) and bare soil (g_{bs}) surfaces:

$$g_T = f_v g_v + (1 - f_v) g_{bs}, \quad (10)$$

where f_v is the vegetated fraction of the grid cell calculated from normalized difference vegetation index (NDVI) observations using the approach of Choudhury et al. (1994):

$$f_v = 1 - \left(\frac{NDVI - NDVI_{min}}{NDVI_{max} - NDVI_{min}} \right)^p. \quad (11)$$

Parameters $NDVI_{min}$ and $NDVI_{max}$ represent the maximum range of NDVI observations within a scene.

Despite these modifications, TOPLATS retains a relatively simple single-layer energy balance formulation since neither the vertical divergence of radiation through the canopy nor the lateral coupling of vegetation and soil energy fluxes is represented. Following Norman et al. (1995), separate T_{aero} predictions over sub-pixel areas of vegetation and bare soil are integrated into an estimate of bulk surface radiometric temperature (T_s) via:

$$T_s \approx (f_v T_{aero,veg}^4 + (1 - f_v) T_{aero,soil}^4)^{0.25}. \quad (12)$$

3. Model application to SMACEX

Intensive data collection efforts during SMACEX provide much of the ancillary data required to force and parameterize each model. Both TOPLATS and the TSEB model were run on a 60-m grid within the entire domain shown in Figure 1. The TSEB model was run on cloud-free Thematic Mapper (TM) images acquired at 1630 UTC 23 June, 1645 UTC 1 July and 1650 UTC 8 July 2002. TOPLATS moisture states were initialized using observations from the United States Department of Agriculture (USDA) Surface Climate Analysis Network (SCAN) site at Ames, Iowa and run on a hourly time step from 0100 UTC 15 June 2002 until 2300 UTC 13 July 2002.

3.1. Model validation data

Model energy flux predictions were evaluated using tower-based eddy covariance observations described in Preuger et al. (this issue). Eddy covariance sensors were mounted on towers at roughly twice the canopy height and adjusted periodically as crop canopy heights increased. Measurements were acquired at a sampling frequency of 20 Hz and passed through a low-pass filter to compute 30-minute flux averages. Tower sites were evenly distributed among corn and soybean fields and sited away from land cover transitions (Figure 1). As with most eddy covariance systems, the sum of turbulent ($H + LH$) and ground heat flux measurements (G) observations at these towers during SMACEX was generally less than observed net radiation (Rn). Based on comparisons with independent aircraft observations during SMACEX, there are some indications the closure problems may manifest themselves more in LH eddy covariance observations

than in H (Preuger et al., this issue). This is consistent with earlier work based on the intercomparison of eddy covariance and Bowen ratio flux observations (Brotzge and Crawford, 2003). Consequently, all flux tower measurements presented here were derived via closing the observed energy balance through the calculation of LH as a residual ($LH = Rn - H - G$). However, since definitive evaluation of various closure techniques is not possible, instances in which our choice of closure strategy may impact model results are noted in Section 4.

Identifying the upwind source area (i.e. fetch) for flux tower measurements is often a source of error in intercomparison between distributed modeling results and tower observations. Here, flux tower observations are compared against averaged values for all 60-m modeling pixels whose center fall within a 150-m square box located immediately up-wind from a given tower. Analysis of SMACEX flux tower observations using more sophisticated fetch modeling suggests that this is a reasonable approximation (Li et al., 2005). Because SMACEX was run in tandem with the 2002 Soil Moisture Experiment (SMEX02), extensive ground-based soil moisture observations are also available for validation. A full evaluation of TOPLATS soil moisture and streamflow predictions during the SMACEX period is described in Crow et al. (2005).

3.2. Model forcing and parameterization data

For the three TM overpass times, values of leaf area index (LAI) and plant height (h) were derived from Thematic Mapper (TM) observations of the normalized difference water index (NDWI) and empirical models presented in Anderson et al. (2004). For

TOPLATS time steps between cloud-free TM overpasses, parameter values were based on the linear interpolation of these estimates. Roughness lengths for momentum and heat transfer were assumed to $h/8$, and zero plane displacement height (D) was set to $2h/3$. Air temperature, vapor pressure, and wind speed observations on 23 June and 1 July came from 40-m Twin Otter aircraft observations. When aircraft data was unavailable, meteorological forcing data were derived from approximately 2-m observations at ground-based stations shown in Figure 1. Both models used measurement height inputs to adjust for vertical differences between aircraft and tower-based measurements. With the exception of rainfall inputs for TOPLATS, all meteorological observations were spatially averaged into a single value for the entire domain.

Application of the TSEB model to SMACEX conditions is fully described in Li et al. (this issue). All TSEB model results are based on the series version of the TSEB model (Norman et al., 1995) and the application of the vegetation clumping correction presented in Kustas and Norman (1999b). Net radiation forcing for the TSEB (not required as an input for TOPLATS) was calculated using tower-based observations of downward solar radiation and the approach of Campbell and Norman (1998).

Precipitation observations for TOPLATS were taken from National Center for Environmental Prediction (NCEP) 4-km merged radar/gauge Stage IV precipitation products. Soil texture maps of the region were derived from the Iowa State Soil Properties and Interpretation Dataset created by Iowa State University in cooperation with the USDA and Iowa Department of Agriculture and Land Stewardship. Values

of Z_{eff} , defined as the depth above which 80% of plant roots are found, were based on consideration of corn and soybean growth stage during the experiment and typical seasonal root development for both crops. Over the course of the experiment Z_{eff} values for soybean increased from 0.3 to 0.6 m and from 0.6 to 0.75 meters for corn. Relative fractions of rooting area in each of the model's four vertical soil layers were calculated by assuming an exponential decay of root area density with depth. Following Feddes (1972), the root spacing parameter α in (8) was defined to using the empirical relationship $0.0013/Z_{eff}$ where both Z_{eff} and α are in meters. Fractional vegetation cover (f_v) was derived using (11) and cloud-free Thematic Mapper (TM) imagery acquired on 23 June and 1 July 2002. A value of 2.5×10^8 s was used for both soybean and crop r_p . This is somewhat lower than typically cited values of between 5×10^8 and 1×10^9 s for crops (Wetzel and Chang, 1987) and must be considered a tuned parameter. The impact of this tuning will be discussed in Section 4.2.2. Due to a lack of site-specific measurements, the albedo and emissivity of all modeled land surfaces were set to 0.20 and 0.96, respectively. All soil parameters were derived from the soil textural classification map and the texture-based lookup tables presented in Cosby et al. (1984). Based on comparison with LAI measurements during SMACEX, optimal values for $NDVI_{max}$, $NDVI_{min}$, and p in (11) were found to be 0.93, 0.037, and 0.606 respectively (M. Anderson, personal communication).

In addition to corn and soybean fields, smaller areas of grass, tree, and urban landcover are present within the modeling domain. No distinction was made between grass and agricultural crops. Trees were distinguished by using a deeper Z_{eff} (1-m) and

increasing r_p to 1.5×10^9 s. Urban areas were treated the same as vegetated pixels, except they were modeled as impermeable (via specification of an extremely low hydraulic conductivity) and their characteristic lack of biomass was captured by TM-based *LAI* images of the region.

4. Results

Results focus on evaluating energy flux results from both approaches (TOPLATS and the TSEB model) using eddy covariance flux-tower measurements made during the SMACEX field campaign. Section 4.1 focuses on evaluating spatially explicit patterns of surface energy fluxes predicted by both models, and Section 4.2 examines the potential for using intercomparison results to improve model results via simple error filtering and/or model calibration techniques.

4.1. Model Intercomparison

Figure 2 shows domain-averaged energy flux, surface temperature, and soil moisture results for TOPLATS during the SMACEX period. Prior to 4 July, there is a notable lack of precipitation and a steady reduction in surface soil moisture. Comparisons with SMEX02 soil moisture observations indicate that TOPLATS is accurately capturing soil moisture dynamics within this time period (Crow et al., 2005). TOPLATS latent heat flux (*LH*) predictions during the dry-down are nearly constant and seem to reflect a rough equilibrium between increasing vegetation cover (tending to increase *LH*) and decreasing soil moisture (tending to decrease *LH*). The dry-down is interrupted by a

series of precipitation events between 4 and 10 July. These events increase soil moisture and decrease predicted levels of H , T_s , and G . The steady decrease in G predictions throughout the period also reflects the reduction of radiation incident on the soil surface due to the seasonal development of crop canopies.

Equivalent TSEB model energy flux predictions are available for the three TM overpass times (1630 UTC 23 June 2002, 1645 UTC 1 July 2002, and 1650 UTC 8 July 2002). Spatial imagery of TOPLATS and TSEB model LH and H predictions at all three times (Figures 3 and 4) reveal significant differences between flux predictions made by the models. Relative to the TSEB model, TOPLATS yields larger (smaller) LH (H) estimates on 23 June (Figures 3 and 4) and predicts significantly more spatial variation in LH on 8 July (Figure 3). Spatial variability in 8 July TOPLATS flux predictions is driven largely by variations in crop type with higher LH predicted for corn fields relative to soybean fields. The TSEB model generally tends to predict smaller corn/soybean contrasts, especially for wet conditions on 8 July. Relative to the TSEB model, TOPLATS also predicts somewhat lower H values for corn fields on 1 July..

The accuracy of TOPLATS and TSEB model energy flux predictions in Figures 3 and 4 can be evaluated through comparison with available flux tower observations. Figure 5 plots the average for flux-tower observations of LH and H against the average of all TOPLATS grid-cells within the estimated fetch of any flux tower. Since tower-based observations of G and T_s in Figure 5 are essentially point-scale measurements, TOPLATS results for these variables are based on averaging model estimates for the 60-m pixel closest to each tower location. TOPLATS appears to

demonstrate a reasonable level of skill in predicting temporal trends in energy fluxes and T_s . Nevertheless, several shortcomings in TOPLATS predictions are apparent. TOPLATS under-predicts LH from roughly 2 July onward. Underpredicting LH excessively heats the surface and results in the over-prediction of T_s during the same time period. TOPLATS also under-predicts H throughout the experiment. It is worth noting that energy flux observations in Figure 5 are closed by solving for LH as the residual of Rn , H and G measurements. Closure via preservation of the observed Bowen Ratio (H/LH) would raise observed H slightly (up to 50 Wm^{-2}) and exacerbate the low bias in TOPLATS H predictions.

The dotted vertical lines in Figure 5 represent TM overpass times when TSEB model predictions of surface energy fluxes are also available. Figure 6 shows scatter plots for TSEB and TOPLATS energy flux predictions against flux tower observations at these overpass times. As in Figure 5, TSEB and TOPLATS pixels are flux-averaged results. Despite problems noted in Figure 5, TOPLATS LH predictions for the three TM overpasses times are reasonably accurate and demonstrate a root-mean-square (RMS) error of 67 Wm^{-2} . This is slightly larger than the RMS error of 63 Wm^{-2} calculated for TSEB model LH predictions. However, the excessive spread of TOPLATS LH predictions relative to observations on 8 July implies that TOPLATS is over-emphasizing variability due to corn/soybean vegetation contrasts. On 8 July, TOPLATS LH predictions in corn fields are biased high by 59 Wm^{-2} and TOPLATS soybean LH predictions are biased low by 97 Wm^{-2} in soybean fields. Since corn tends to transpire more than soybeans (due to higher LAI values) these biases combine

to exaggerate the magnitude of LH differences observed in corn and soybean fields. TSEB model H predictions in Figure 6 are significantly more accurate than comparable TOPLATS predictions - demonstrating a RMS error of 22 Wm^{-2} versus 46 Wm^{-2} for TOPLATS. A significant fraction of TOPLATS H error is due to a pronounced low bias in H predictions on 23 June.

4.2. Improving Model Performance

When combined with extensive SMACEX flux tower observations, TOPLATS and TSEB results in Section 4.1 can be used to evaluate prospects for designing error filtering and/or model calibration techniques to merge instantaneous RS-SVAT model predictions with continuous WEB-SVAT results.

4.2.1. Linear filtering. The successful filtering of errors in WEB-SVAT flux results via the assimilation of RS-SVAT predictions requires that modeling errors in both approaches be substantially independent. During SMACEX, the strategy used for estimating spatial patterns of LH and H by both models are sufficiently different that concurrent energy flux errors in TOPLATS and TSEB model predictions are essentially independent (Figure 7). Figure 8 demonstrates a simple example of filtering via linear weighted averaging of TOPLATS and TSEB results for a range of weight on TOPLATS predictions $W_{TOPLATS}$ ($W_{TSEB} = 1 - W_{TOPLATS}$). Due to the mutual independence of modeling errors, almost any weighted combination of TOPLATS and TSEB LH results provides a filtered flux estimate that is superior, in an RMS sense, to either model in isolation. An optimal choice of $W_{TOPLATS}$ near 0.5 is capable of filtering

nearly one-third of LH error in both models. Since linear averaging - with variable weights determined from model and observation error/covariance information - is the basis of most sequential data assimilation techniques, LH results in Figure 8 provide important theoretical support for more complex data assimilation schemes aimed at the integration of WEB- and RS-SVAT LH predictions. However, because TOPLATS H predictions exhibit a negative bias and are significantly less accurate than comparable TSEB predictions, H results obtained by weighted averaging improve upon TSEB H predictions only for small values of $W_{TOPLATS}$ and then only marginally. That is, TSEB H results have clear value for improving TOPLATS H predictions but not vice versa.

4.2.2. Model calibration. The simple linear averaging procedure shown in Figure 8 is effective for filtering LH errors but possible only for isolated times in which remotely-sensed observations of T_s are available. An alternative possibility is the development of model calibration approaches based on the intercomparison of continuous TOPLATS predictions with either instantaneous RS-SVAT flux predictions (e.g. Franks and Beven, 1999) or the T_s observations underlying RS-SVAT predictions (e.g. Crow et al., 2003). Figure 9 establishes the basis for both approaches during SMACEX by plotting differences between TOPLATS and TSEB model predictions (Figure 9a and 9c) and TOPLATS T_s predictions and satellite-based (TM) T_s observations (Figures 9b and 9d) against absolute errors in TOPLATS turbulent flux predictions during the three TM overpass times. All quantities plotted in Figure 9 are based on averaging within the assumed tower fetch area (see Section 3.1). Provided periodic remote observations of T_s are available, quantities plotted on the x-axis of Figure 9 will be

available in an operational setting. The existence of a significant correlation in Figure 10 suggests that TOPLATS flux errors (plotted on the y-axis) can be diagnosed via TOPLATS/TSEB flux differences and/or TOPLATS/satellite T_s differences plotted on the x-axis. A calibration strategy would exploit this correlation, and improve TOPLATS flux predictions (on the y-axis), by adjusting model parameters to minimize observed differences (on the x-axis). It should be noted that plots involving TOPLATS/satellite T_s differences (Figures 9b and 9d) do not appear to trend exactly through the origin. Consequently, complete removal of TOPLATS/satellite T_s differences via calibration may result in a positive (negative) bias for calibrated TOPLATS LH (H) predictions. An analogous problem does not appear to exist for calibration against TSEB flux predictions (Figures 9a and 9c).

Over vegetated areas, WEB-SVAT models make predictions about the onset of water stress based on set of calculations concerning soil moisture levels and the availability of this water for plant uptake. These calculations can exhibit sensitivity to highly uncertain parameter values governing root water uptake, vertical water flow within the root zone, and estimates of soil water levels associated with the onset of water stress. For example, increasing the plant resistivity value r_p used in (7) from the value of 2.5×10^8 s - used for all previous TOPLATS results presented here - to 7.5×10^8 s leads to a significant reduction in TOPLATS LH predictions between 30 June and 3 July by restricting the ability of roots to draw water from deep soil layers and compensate for the drying of surface layers. This restriction causes TOPLATS to sharply under-predict LH values during this period. This sensitivity is significant given uncertainties in the

correct value of r_p for various agricultural crops.

The response to variations in the r_p parameter illustrates a common problem in WEB-SVAT modeling whereby model predictions exhibit sensitivity to parameter values that are poorly known. The only viable solution in such circumstances is to develop model calibration techniques that allow parameter values to be derived from the calibration of model output against available observations. Figure 10 presents a simple calibration example where errors in TOPLATS LH predictions observed at flux tower sites on 1 July are plotted against observed TOPLATS T_s errors and observed differences between TOPLATS and TSEB LH predictions for a range of r_p values. The first day of July is chosen since it covers the driest period in the experiment and the period of highest sensitivity of TOPLATS flux results to r_p . Both plots demonstrate a significant level of correlation and suggest that the selection of parameters which minimize observable quantities on the x-axis will also minimize RMS error in TOPLATS LH predictions. For example, using a typical literature value of 7.5×10^8 s for all corn and soybean fields (solid triangles in Figure 10) yields an LH RMS error of 141 Wm^{-2} on 1 July. However, individually selecting r_p parameters for each flux tower site that minimize the difference between either TOPLATS and satellite T_s (Figure 10a) or TOPLATS and TSEB LH (Figure 10b) reduces TOPLATS RMS error to 51 and 41 Wm^{-2} , respectively. Calibrated values of r_p range between 0.5×10^8 and 5.0×10^8 s and offer some justification for the use of 2.5×10^8 s in prior simulations.

5. Discussion and Summary

Both RS- and WEB-SVAT approaches are sufficiently mature to form the basis of independent efforts to operationally monitor the land surface at continental scales (see Mitchell et al. (2004) for WEB-SVAT modeling and Diak et al. (2004) for RS-SVAT modeling efforts). Despite these advances, relatively little work has been done at intercomparing surface energy flux predictions made by each model type. This study underscores differences between the two approaches and describes the potential benefits of integrating them.

Visual intercomparison of surface flux results (Figures 3 and 4) reveals significant differences between predictions of turbulent energy fluxes during SMACEX made by a RS-SVAT model (TSEB) and a WEB-SVAT model (TOPLATS). These differences are interpreted using extensive flux tower observations available during SMACEX. TOPLATS energy flux predictions are able to reproduce temporal trends in spatially-averaged energy flux values (Figure 5) but cannot match the accuracy of the TSEB model in predicting instantaneous H and LH magnitudes at specific tower sites (Figure 6). The most serious shortcoming in TOPLATS H predictions is a low bias on 23 June (Figures 5) and a tendency, relative to both TSEB predictions (Figure 3) and tower observations (Section 4.1), to over-estimate flux contrasts between corn and soybean fields. The over-prediction of corn/soybean contrasts appears especially stark on 8 July following a period of extensive rainfall. This tendency is not surprising given that the TSEB model has access to a spatially explicit observations of T_s to guide flux

predictions while TOPLATS is forced to rely solely on explicit maps of vegetation type and uncertain rainfall observations in order to produce spatially distributed energy flux maps.

Nevertheless, WEB-SVAT models like TOPLATS have two distinct advantages over RS-SVAT approaches. First, they are able to make temporally continuous predictions and are not limited by the sporadic availability of remote T_s observations. Second, they are able to predict soil moisture and sub-surface soil temperature states which are critical for a number of key applications for SVAT models including the initialization of numerical weather prediction models and monitoring of soil water resources in agricultural areas. Given that TSEB predictions are generally more accurate and/or robust to parameterization uncertainties (Figure 6 and Section 4.2.2), a logical extension of model intercomparison results is the development of techniques that use diagnostic TSEB flux predictions to update static TOPLATS parameters via model calibration or data assimilation techniques.

A critical prerequisite for any data assimilation technique aimed at filtering WEB-SVAT errors using RS-SVAT energy flux predictions is the mutual independence of errors in flux estimates made by both models. If flux errors are highly correlated, RS-SVAT predictions will have little value for filtering WEB-SVAT modeling errors. Figure 7 demonstrates that RS- and WEB-SVAT modeling approaches are sufficiently distinct so as to produce essentially independent flux estimate errors. This demonstrates that operational efforts centered on both RS-SVAT and WEB-SVAT approaches may realize immediate benefits via simple linear averaging of energy flux predictions (Figure

8). It also confirms the theoretical basis of previous efforts to sequentially assimilate RS-SVAT model predictions into WEB-SVAT approaches (Schuurmans et al. 2003). In addition to data assimilation, a second possibility for integrating WEB- and RS-SVAT predictions is a model calibration approach that attempts to improve the complex parameterization required for WEB-SVAT models. Figure 9 establishes the feasibility of this approach during SMACEX by demonstrating the potential of improving TOPLATS flux measurements relative to tower observations via a data calibration approach relying on either TSEB LH predictions or satellite T_s observations. Figure 10 presents a simple example of such calibration using an important TOPLATS rooting parameter. A key unanswered question is whether it is advantageous to calibrate TOPLATS using direct T_s observations (Figure 10a) or utilize RS-WEB flux predictions derived from such observations (Figure 10b). Both approaches demonstrate merit during SMACEX.

It should be noted that, as defined here, RS-SVAT and WEB-SVAT are extremely broad terms covering a wide range of modeling approaches. In particular, variations in energy flux predictions between WEB-SVAT approaches are known to be large. Care should therefore be taken when extrapolating results beyond the two specific models (TOPLATS and the TSEB model) examined here. Further study is also required to determine if results presented here are applicable to RS- and WEB-SVAT modeling strategies currently employed at coarser spatial scales (> 10 km) in operational settings.

References

- Anderson, M.C., J.M. Norman, G.R. Diak, W.P. Kustas, J.R. Mecikalski, 1997: A two-source time-integrated model for estimating surface fluxes from thermal infrared satellite observations. *Remote Sens. Environ.*, **60**, 195–216.
- Anderson, M.C., C.M. Neale, F. Li, J.M. Norman, W.P. Kustas, H. Jayanthi, and J. Chavez, 2004: Upscaling ground observations of vegetation cover and water content during SMEX02 using aircraft and Landsat imagery. *Remote Sens. Environ.*, **90**(4), 447–464.
- Bastiaanssen, W., M. Menenti, R. Feddes, and A. Holtslag, 1998: A remote sensing surface energy balance algorithm for land (SEBAL) 1. Formulation. *J. Hydrol.*, **212-213**, 198–212.
- Bindlish, R., W.P. Kustas, A.N. French, G.R. Diak, and J.R. Mecikalski, 2001: Influence of near-surface soil moisture on regional scale heat fluxes: Model results using microwave remote sensing data from SGP97. *IEEE Trans. Geosci. Remote Sensing*, **39**, 1719-1728.
- Brotzge, J.A. and K.C. Crawford, 2003: Examination of the surface energy budget: A comparison of eddy correlation and Bowen ratio measurement systems. *J. Hydrometeor.*, **4**, 160–178.
- Campbell, G.S., and J.M. Norman, 1998: *An Introduction to Environmental Biophysics*, Springer-Verlag, New York, 286 pp.
- Castelli, F., D. Entekhabi, and E. Caporali, 1999: Estimation of surface heat flux and an

- index of soil moisture using adjoint-state surface energy balance. *Water Resour. Res.*, **35**, 3115–3125.
- Choudhury, B.J., N.U. Ahmed, S.B. Idso, R.J. Reginato, and C. Daughtry, 1994: Relations between evaporation coefficients and vegetation indices studied by model simulations. *Remote Sens. Environ.*, **50**, 1–17.
- Cosby, B. J., G. M. Hornberger, R. B. Clapp, and T. R. Ginn, 1984: A statistical exploration of the relationships of soil moisture characteristics to the physical properties of soils. *Water Resour. Res.*, **20**, 682–690.
- Crow, W.T., E.F. Wood, and M. Pan, 2003: Multi-objective calibration of land surface model evapotranspiration predictions using streamflow observations and spaceborne surface radiometric temperature retrievals. *J. Geophys. Res.*, **108**(D23), doi:10.1029/2002JD003292.
- Crow, W.T., D. Ryu, and J.S. Famiglietti, 2005: Upscaling of field-scale soil moisture measurements using distributed land surface modeling. In press, *Adv. Water Resour.*
- Dai, Y., and Coauthors, 2003: The Common Land Model (CLM). *Bull. Amer. Meteor. Soc.*, **84**, 1013–1023.
- Diak, G.R., Mecikalski, J.R. , Anderson, M.C., Norman, J.M., Kustas, W.P., Torn, R.D., and DeWolf R.L., 2004: Estimating land surface energy budgets from space: Review and current efforts at the University of Wisconsin-Madison and USDA-ARS. *Bull. Amer. Meteor. Soc.*, **85**, 65–78.

- Famiglietti, J.S., and E.F. Wood, 1994: Multiscale modeling of spatially variable water and energy balance processes. *Water Resour. Res.*, **30**, 3061–3078.
- Feddes, R.A. and P.E. Rijkema, 1972: Water withdrawal by plant roots. *J. Hydrol.*, **17**, 33–59.
- Franks, S.W., and K.J. Beven, 1999: Conditioning a multi-patch SVAT model using uncertain time-space estimates of latent heat fluxes as inferred from remotely-sensed data. *Water Resour. Res.*, **35**, 2751–2761.
- French, A.N., T.J. Schmugge, W.P. Kustas, K.L. Brubaker, and J. Prueger, 2003: Surface energy fluxes over El Reno, Oklahoma using high-resolution remotely sensed data. *Water Resour. Res.*, **39**, doi:10.1029/2002WR001734.
- Goudriaan, J., 1977: *Crop Micrometeorology: A Simulation Study*. Center for Agric. Publ. and Doc., Wageningen, The Netherlands, 249 pp.
- Gupta, H.V., L.A. Bastidas, S. Sorooshian, W.J. Shuttleworth, and Z.L. Yang, 1999: Parameter estimation of a land surface scheme using multicriteria methods. *J. Geophys. Res.*, **104**, 19491–19503.
- Henderson-Sellers, A., P. Irannejad, K. McGuffie, and A.J. Pitman, 2003: Predicting land-surface climates-better skill or moving targets? *J. Geophys. Lett.*, **30**(14), doi:10.1029/2003GL017387.
- Jiang, L., and S. Islam, 2001: Estimation of surface evaporation map over southern Great Plains using remote sensing data. *Water Resour. Res.*, **37**, 329–340.

- Koster, R.D., M.J. Suarez, A. Ducharne, M. Stieglitz, and P. Kumar, 2000: A catchment-based approach to modeling land surfaces processes in a general circulation model, 1: Model structure. *J. Geophys. Res.*, **105**(20), 24809–24822.
- Kustas, W.P., and J.M. Norman, 1996: Use of remote sensing for evapotranspiration monitoring over land surfaces. *Hydrolog. Sci. J.*, **41**, 495–516.
- Kustas, W.P., and J.M. Norman, 1997: A two-source approach for estimating turbulent energy fluxes using multiple angle thermal infrared observations. *Water Resour. Res.*, **33**, 1495–1508.
- Kustas, W.P., Zhan, X., and Schmugge, T.J, 1998: Combining optical and microwave remote sensing for mapping energy fluxes in a semiarid watershed. *Remote Sens. Environ.*, **64**, 116–131.
- Kustas, W.P., and J. M. Norman, 1999a: Reply to comments about the basic equations of dual-source vegetation-atmosphere transfer models. *Agric. For. Meteorol.*, **94**, 275–278.
- Kustas W.P., and J.M. Norman, 1999b: Evaluation of soil and vegetation heat flux predictions using a simple two-source model with radiometric temperature for partial canopy cover. *Agric. For. Meteorol.*, **94**, 13–29.
- Kustas W.P., and J.M. Norman, 2000a: A two-source energy balance approach using directional radiometric temperature observations for sparse canopy covered surfaces. *Agron. J.*, **92**, 847–854.

- Kustas W.P., and J.M. Norman, 2000b: Evaluating the effects of subpixel heterogeneity on pixel average fluxes. *Remote Sens. Environ.*, **74**, 327–342.
- Kustas, W.P, J.L. Hatfield, and J.H. Prueger, 2005: The Soil Moisture Atmosphere Coupling Experiment (SMACEX): Background, hydrometeorological conditions and preliminary findings. *J. Hydrometeor.*, This issue.
- Li, F., W.P. Kustas, J.H. Prueger, C.M.U. Neale and T.J. Jackson, 2005: Utility of remote sensing based two-source energy balance model under low and high vegetation cover conditions. *J. Hydrometeor.*, This issue.
- Liang, X., D. P. Lettenmaier, E. F. Wood, and S. J. Burges, 1994: A simple hydrologically based model of land surface water and energy fluxes for GCMs. *J. Geophys. Res.*, **99**, 14415–14428.
- Mecikalski, J.R., G.R. Diak, M.C. Anderson, and J.M. Norman, 1999: Estimating fluxes on continental scale using remotely-sensed data in an atmospheric-land exchange model. *J. Appl. Meteorol.*, **50**, 221–247.
- Mitchell, K. E., and Coauthors, 2004: The multi-institution North American Land Data Assimilation System (NLDAS): Utilizing multiple GCIP products and partners in a continental distributed hydrological modeling system. *J. Geophys. Res.*, **109**, doi:10.1029/2003JD003823.
- Norman, J. M., Kustas, W. P. and Humes, K. S., 1995: A two-source approach for estimating soil and vegetation energy fluxes in observations of directional radiometric surface temperature. *Agric. For. Meteorol.*, **77**, 263–293.

- Peters-Lidard, C.D., M.S. Zion, and E.F. Wood, 1997: A soil-vegetation- atmosphere transfer scheme for modeling spatially variable water and energy balance processes. *J. Geophys. Res.*, **102**, 4303–4324.
- Pitman, A.J., and Coauthors, 1999: Key results and implications form phase 1(c) of the Project for Intercomparison of Land-surface Parameterization Schemes. *Clim. Dynam.*, **15**, 673–684.
- Priestley, C.H.B., and R. J. Taylor, 1972: On the assessment of surface heat flux and evaporation using large-scale parameters. *Mon. Weather Rev.*, **100**: 81–92.
- Prueger, J.H., J.L. Hatfield, W.P. Kustas, L.E. Hipps, and J.I. MacPherson, 2005, Tower and aircraft eddy covariance measurements of water, energy and carbon fluxes during SMACEX. *J. Hydrometeor.*, This issue.
- Rodell, M, and Coauthors, 2003: The Global Land Data Assimilation System. *Bull. Amer. Meteor. Soc.*, **85**, 381–394.
- Sauer, T.J., J.M. Norman, C.B. Tanner, and T.B. Wilson, 1995: Measurement of heat and vapor transfer at the soil surface beneath a maize canopy using source plates. *Agric. For. Meteorol.*, **75**, 161–189.
- Schuermans, J.M., P. A. Troch, A. A. Veldhuizen, W. G. M. Bastiaanssen, and M. F. P. Bierkens, 2003: Assimilation of remotely sensed latent heat flux in a distributed hydrological model. *Adv. Water. Resour.*, **26**, 151–159.
- Su, Z, 2002: The surface energy balance system (SEBS) for estimation of turbulent heat fluxes. *Hydrol. Earth Syst. Sci.*, **6**, 85–99.

- Wetzel, P.J., and J. Chang, 1987: Concerning the relationship between evapotranspiration and soil moisture. *J. Clim. Appl. Meteor.*, **26**, 18–27.
- Wetzel, P.J., and J. Chang, 1988: Evapotranspiration from nonuniform surfaces: A first approach for short-term numerical weather prediction. *Mon. Weather Rev.*, **116**, 600–621.
- Wood, E.F., and Coauthors, 1998: The Project for Intercomparison of Land-surface Parameterization Schemes (PILPS) Phase 2(c) Red-Arkansas river basin experiment: 1. Experiment description and summary intercomparisons. *Global Planet. Change*, **19**, 115–135.
- Zhan, X., W.P. Kustas, and K.S. Humes, 1996: An intercomparison study on models of sensible heat flux over partial canopy surfaces with remotely sensed surface temperature. *Remote Sens. Environ.*, **58**, 242–256.

W.T. Crow, Hydrology and Remote Sensing Laboratory, USDA ARS, Rm. 104, Bldg. 007, BARC-W, Beltsville, MD 20705.

Received _____

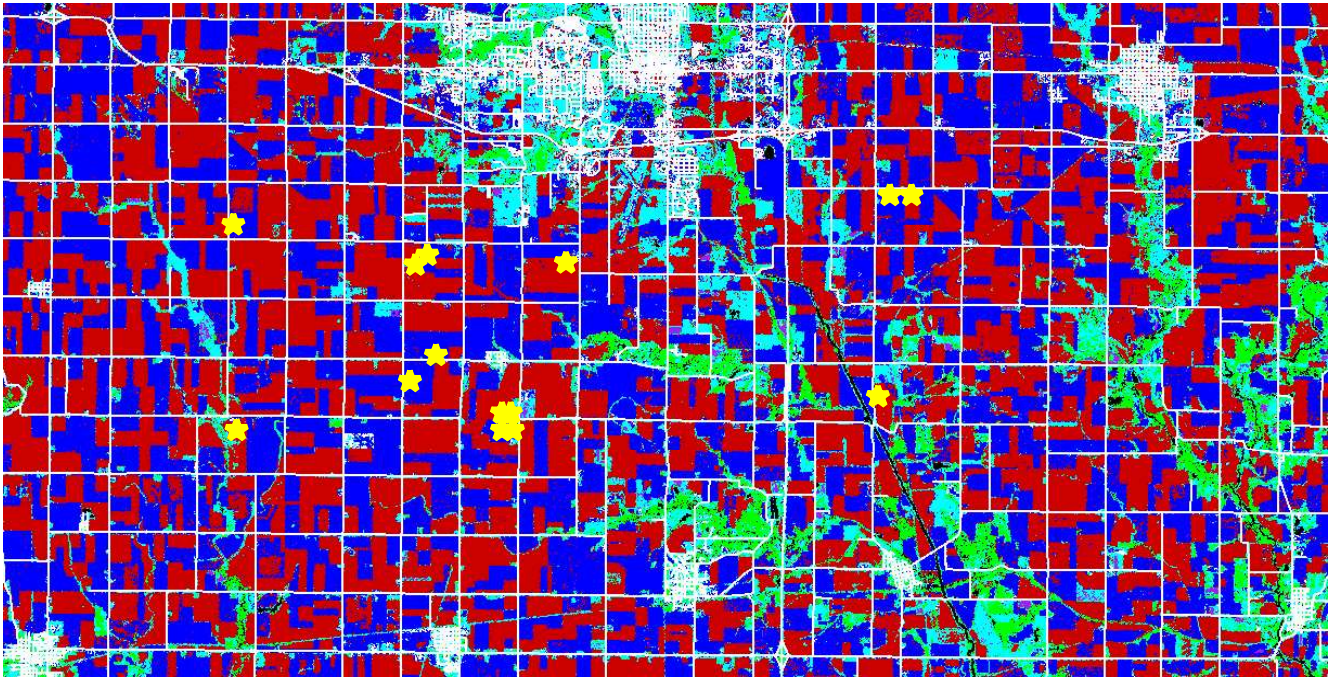


Figure 1: Land-cover classification of modeling domain slightly south of Ames, Iowa. Upper-left corner of image is at 431304 E and 465431 N (NAD83 UTM zone 15). North is upwards. Domain is 36.3 km E-W and 18.4 km N-S. Blue, red, green, white, and cyan denote soybean, corn, tree, urban, and grass areas, respectively. Location of meteorological stations and flux towers are indicated with yellow crosses.

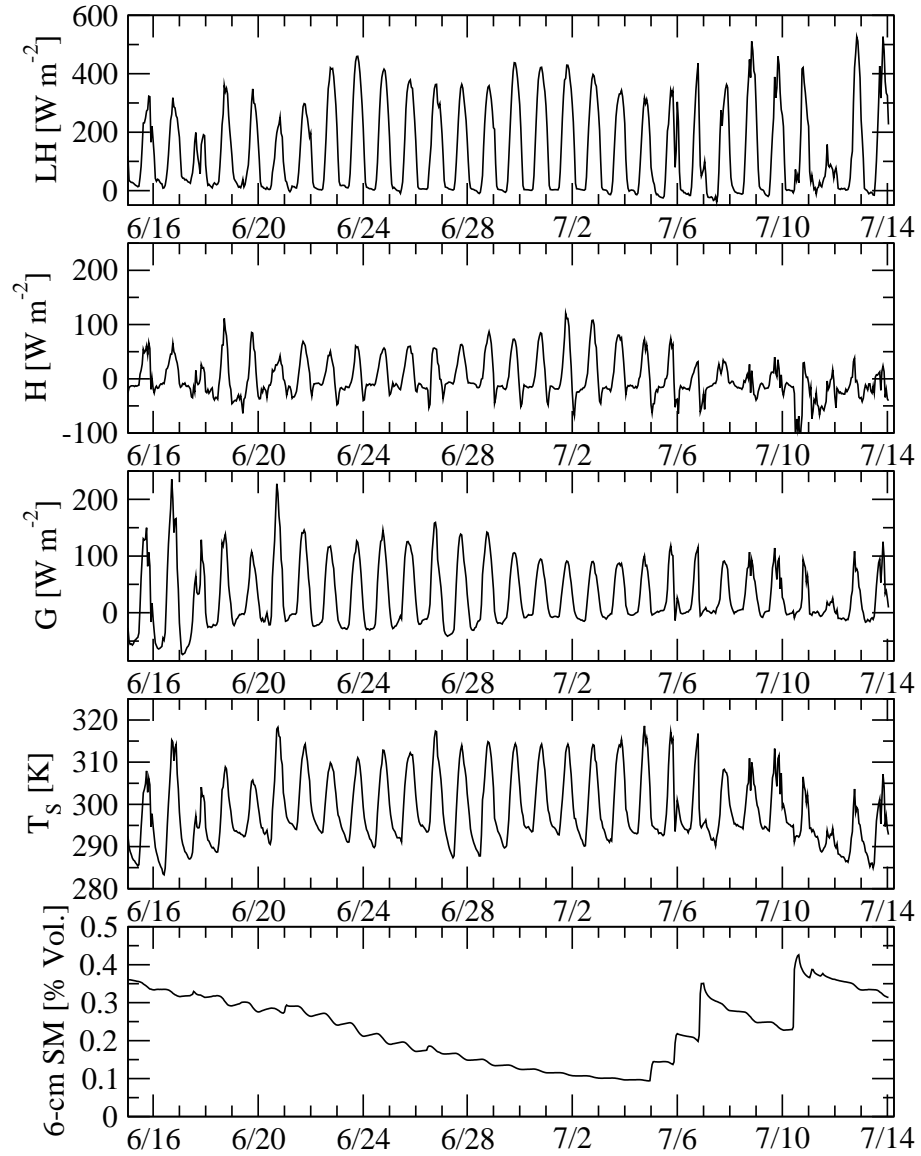


Figure 2: Time series of domain-averaged TOPLATS predictions.

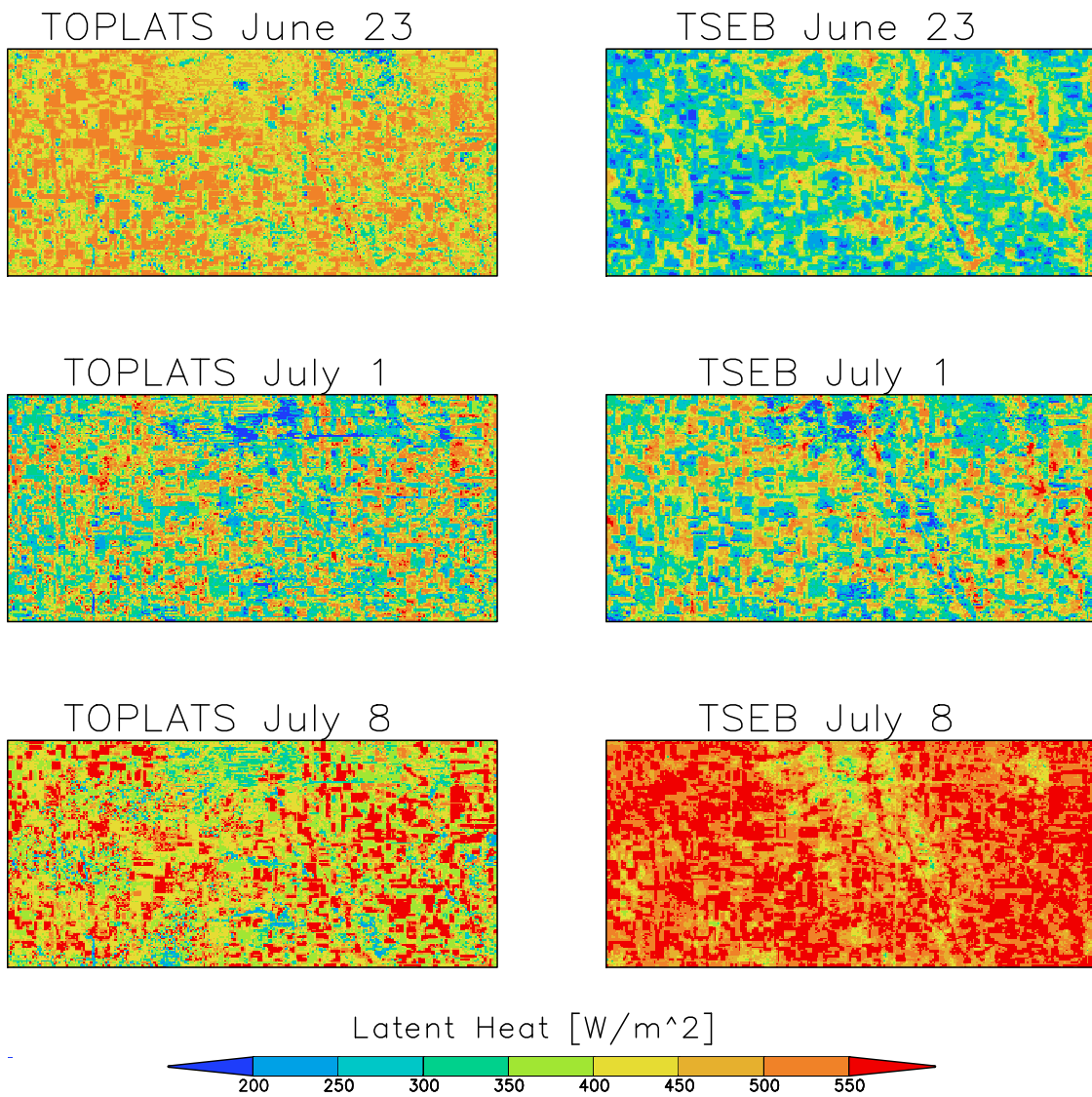


Figure 3: Imagery of TOPLATS and TSEB LH estimates at cloud-free TM overpass times within the modeling domain shown in Figure 1.

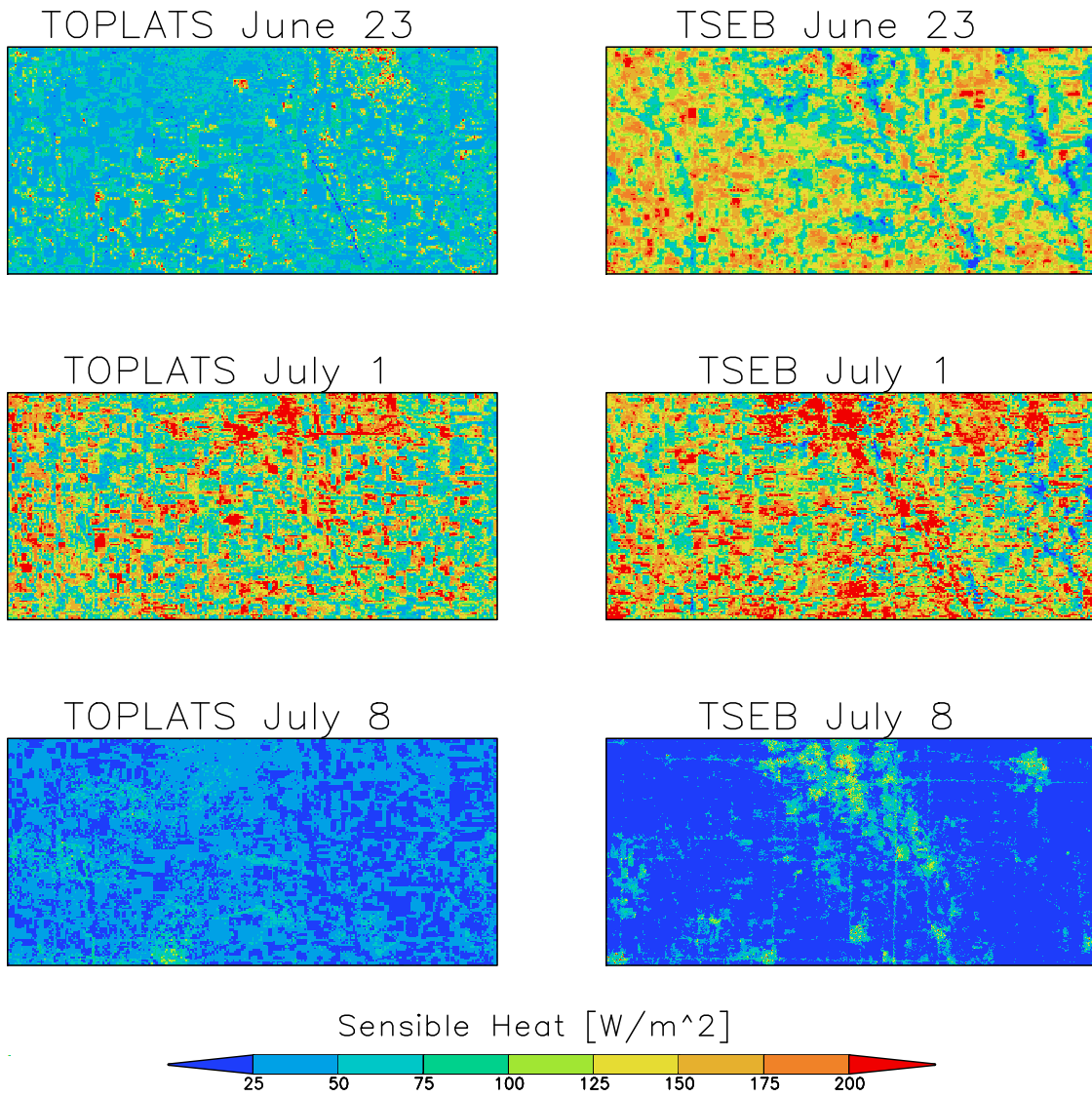


Figure 4: Imagery of TOPLATS and TSEB H estimates at cloud-free TM overpass times within the modeling domain shown in Figure 1.

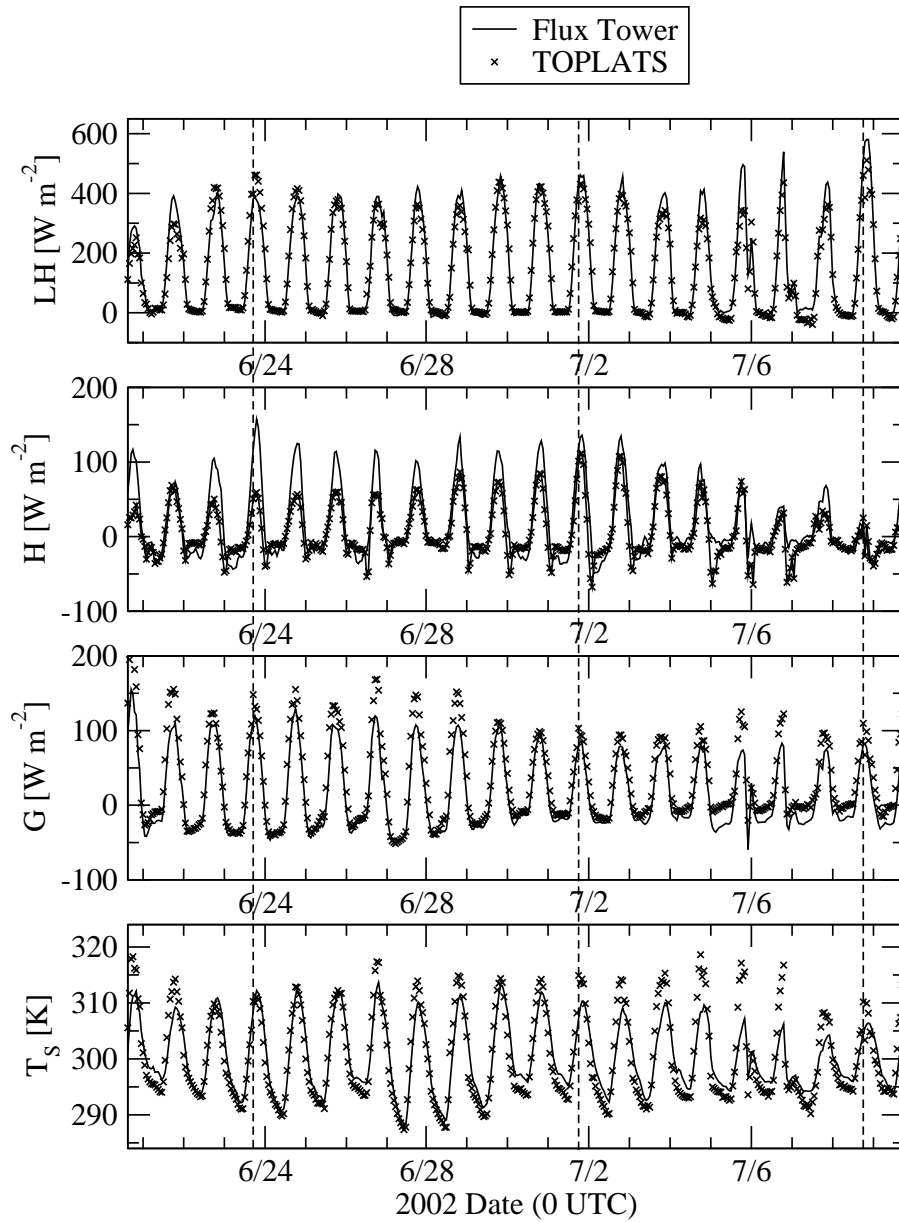


Figure 5: Averaged flux tower LH and H measurements versus average of TOPLATS predictions made within fetch area for flux towers in Figure 1.

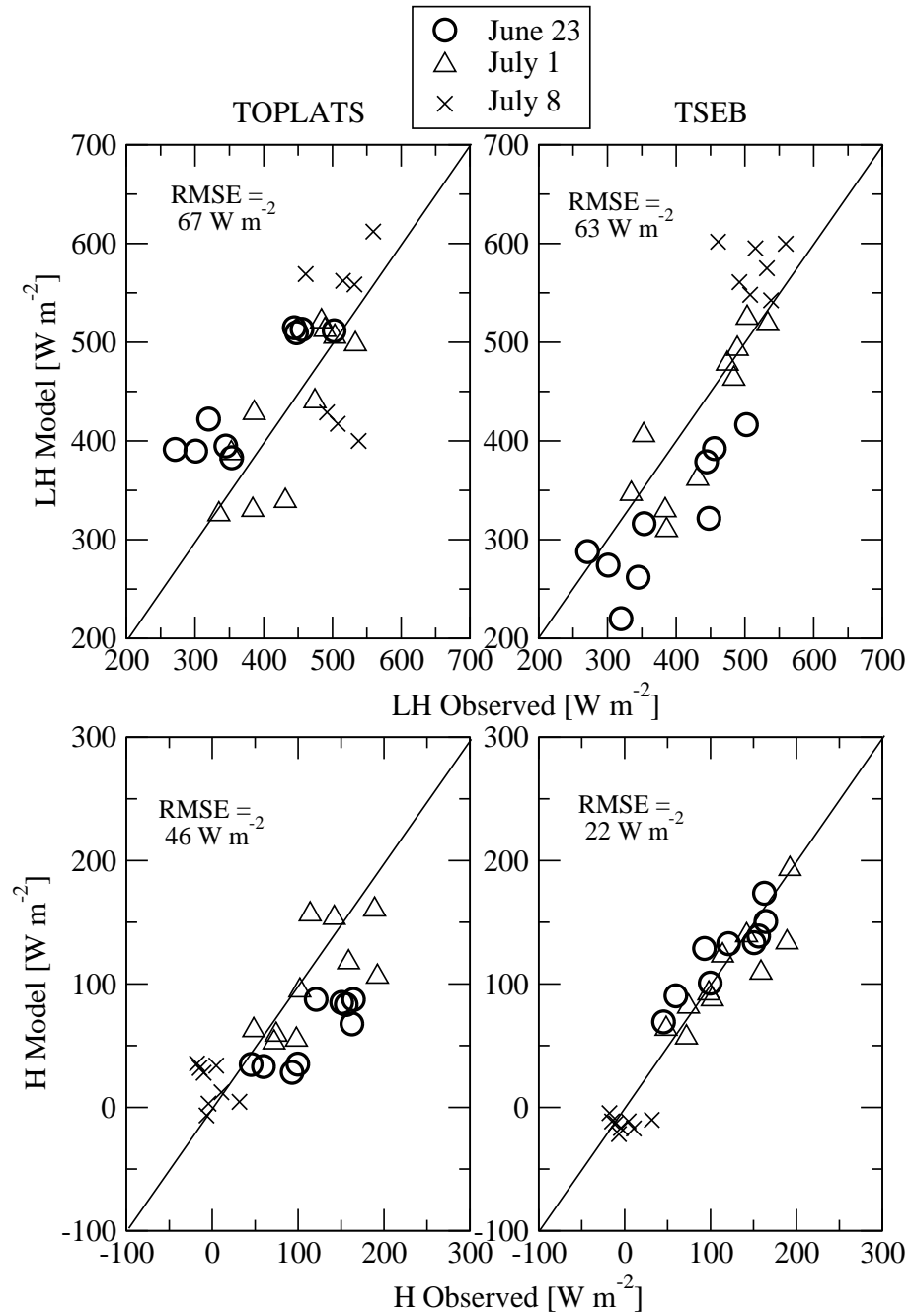


Figure 6: Scatterplots of TOPLATS and TSEB LH and H predictions made within flux tower fetch areas versus flux tower measurements during cloud-free TM overpass times.

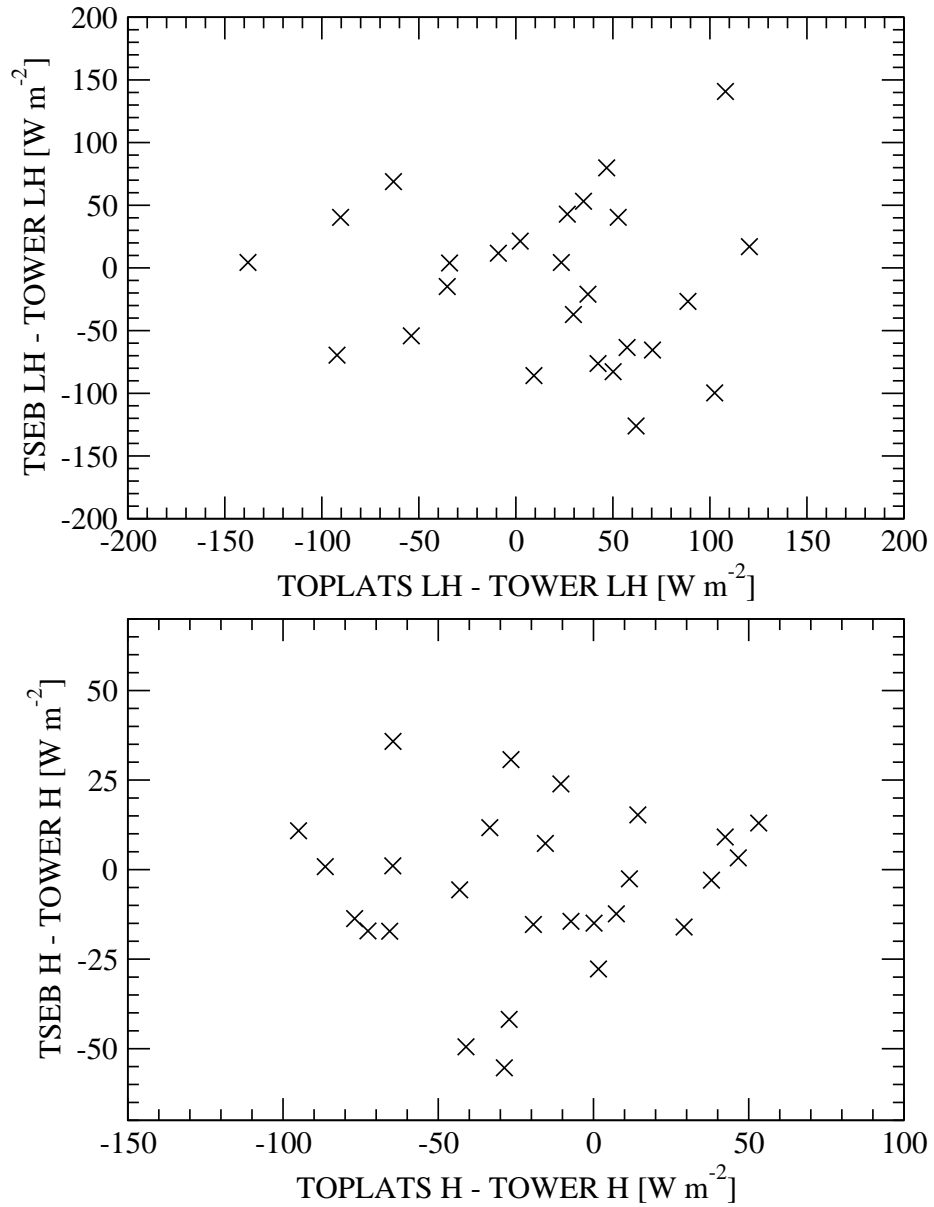


Figure 7: The relationship between TOPLATS and TSEB model LH and H flux estimation errors.

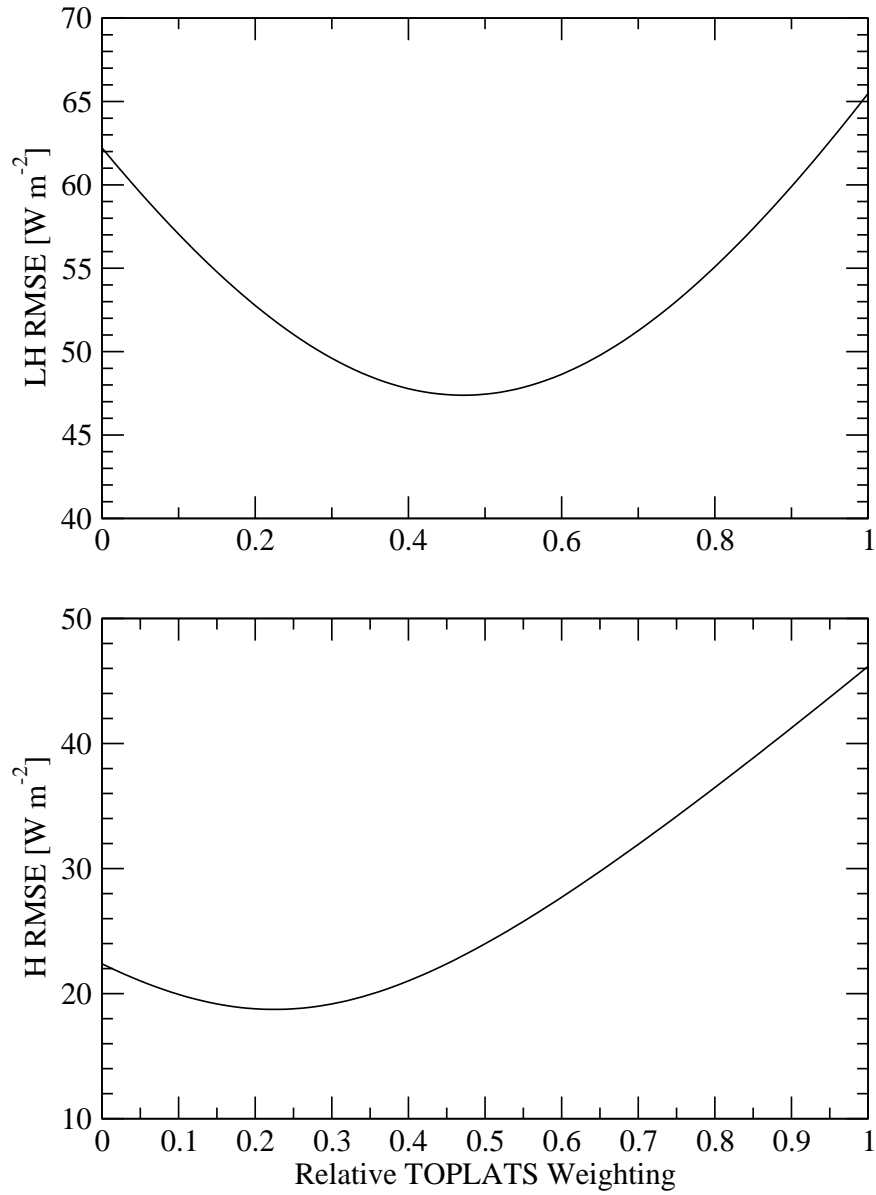


Figure 8: Impact of weighted linear averaging of TOPLATS and TSEB LH and H predictions on flux accuracy for a range of weights.

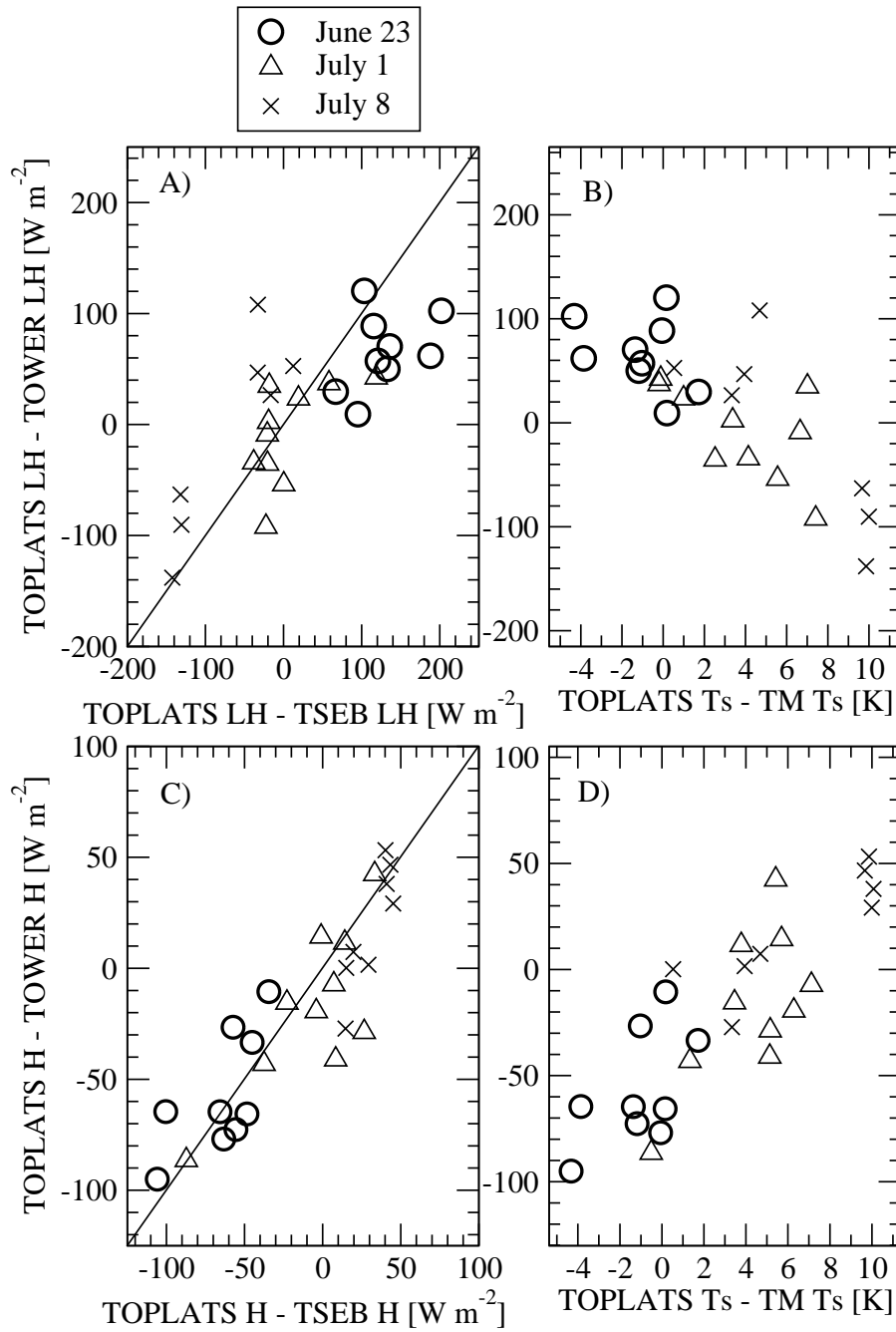


Figure 9: Relationship between TOPLATS LH errors (relative to flux tower observations) and A) differences between TOPLATS and TSEB model LH predictions and B) differences between TOPLATS T_s predictions and satellite (TM) T_s observations. C) and D) are analogous plots except for TOPLATS H errors.

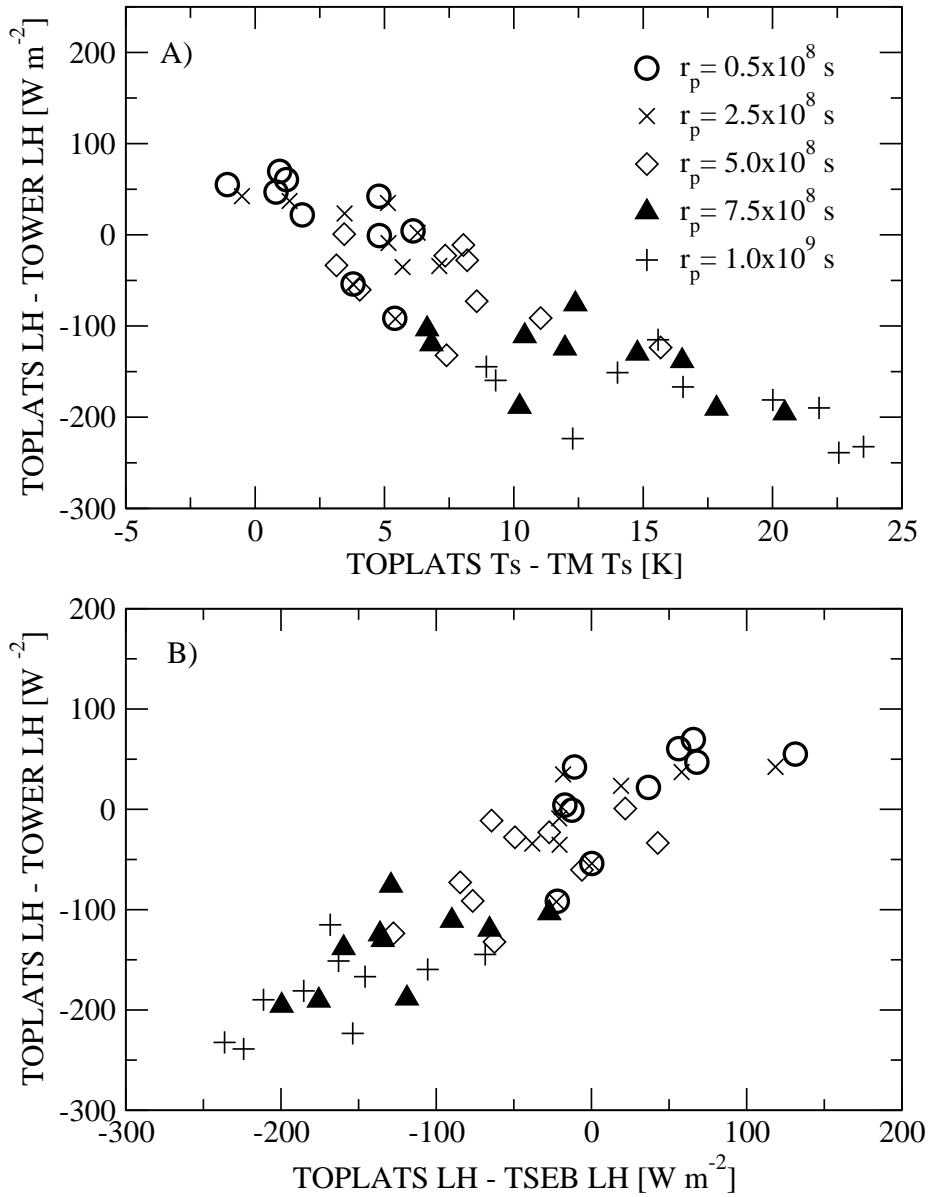


Figure 10: Relationship between 1 July TOPLATS LH errors and A) differences between TOPLATS T_s predictions and satellite (TM) T_s observations, and (B) differences between TOPLATS and TSEB model LH predictions for a range of choices for r_p in (7).